Statistical properties of three-dimensional speckle distributions produced by crossed scattered waves

Takashi Okamoto* and Shuhei Fujita

Department of Systems Design and Informatics, Kyushu Institute of Technology, 680-4, Kawazu, Iizuka, Fukuoka 820-8502, Japan
**Corresponding author: okamoto@ces.kyutech.ac.jp*

Received August 1, 2008; revised October 7, 2008; accepted October 10, 2008; posted October 16, 2008 (Doc. ID 99666); published November 19, 2008

The statistical properties of three-dimensional normal and fractal speckle fields produced by two or three scattered waves crossed orthogonally are studied theoretically. The probability density function and the autocorrelation function of intensity are derived for speckle fields superposed with and without interference. It is shown that the spatial anisotropy of intensity distributions exists even when three scattered waves interfere with one another. This spatial anisotropy affects the power-law distribution of intensity correlation for fractal speckles and leads to intensity patterns that are not self-similar in two or three dimensions. A potential application of the superposed speckle field is proposed. © 2008 Optical Society of America

OCIS codes: 030.6140, 030.6600, 220.3740.

1. INTRODUCTION

Mutually coherent laser beams propagating in different directions can interfere with each other to form a periodic intensity distribution in free space or homogeneous media. Illumination of photoresist or photosensitive polymer with the three-dimensional (3D) interference pattern of light allows us to realize periodic microstructures with high precision. This method is referred to as interference lithography or holographic lithography and is now considered as one of the most promising methods to fabricate photonic crystals [1–4]. The structures can be tailored by changing some parameter values, such as the number of laser beams, their intensities and phases, wave vectors, and polarization vectors. For example, the dimension of periodicity is determined by the number of the laser beams involved.

In interference lithography plane waves are used to produce a simple interference pattern. If such regular waves are scattered by diffusers, the resultant intensity pattern will exhibit a complex random distribution. In addition, if those scattered waves are mutually coherent, the interference pattern will contain periodic fringes, although the overall pattern is random. A combination of the so-called speckle pattern and the above method therefore leads to a new technique for fabricating disordered media.

The above idea has motivated us to study the correlation properties of superposed speckle patterns. The 3D structure of static speckles produced by a single laser beam has already been studied [5]. The speckle structure has been analyzed particularly in terms of spatiotemporal intensity dynamics [6], and the 3D motion of speckle patterns has been elucidated [7–9]. Although there are some investigations on a superposition of speckle patterns arising from separate laser beams [10], the 3D intensity distribution produced by multiple speckle waves has not been fully analyzed yet. In this paper, we investigate the statistical properties of such multiply superposed speckle patterns. In addition to normal speckles produced by illuminating a diffuser with a Gaussian laser beam, we examine the intensity distribution of speckles with fractal properties, which exhibit a power-law correlation of intensity [11]. We derive the analytical expressions for the probability density function and the autocorrelation function of superposed speckle intensity and compare the results with those of a single speckle wave. Potential applications of this new 3D intensity structure are discussed.

2. ANALYTICAL DEVELOPMENT

Figure 1 schematically depicts the optical geometry used for analyzing the superposed speckle field. Three transparent diffusers D_1, D_2, and D_3 are placed at the $\xi\eta$ ($\boldsymbol{\xi}$), $\eta'\zeta'$ ($\boldsymbol{\eta}'$), and $\zeta''\xi''$ ($\boldsymbol{\zeta}''$) planes, and the ξ', η'', and ζ axes are orthogonally crossed at one point to form, respectively, the x, y, and z axes in the observation space. The distances between the origin of the observation space and those of the $\boldsymbol{\xi}$, $\boldsymbol{\eta}'$, and $\boldsymbol{\zeta}''$ planes are L, L', and L'', respectively. Coherent light beams that are mutually coherent are incident normally on D_1, D_2, and D_3. First, we consider a double-wave configuration in which only two scattered waves coming from the $\boldsymbol{\xi}$ and $\boldsymbol{\eta}'$ planes exist, and then we analyze a triple-wave configuration in which another scattered wave from the $\boldsymbol{\zeta}''$ plane is added in the observation space.

A. Superposition of Two Waves

1. Coherent Addition

Let us consider the situation where two light beams linearly polarized in the y direction are incident normally on

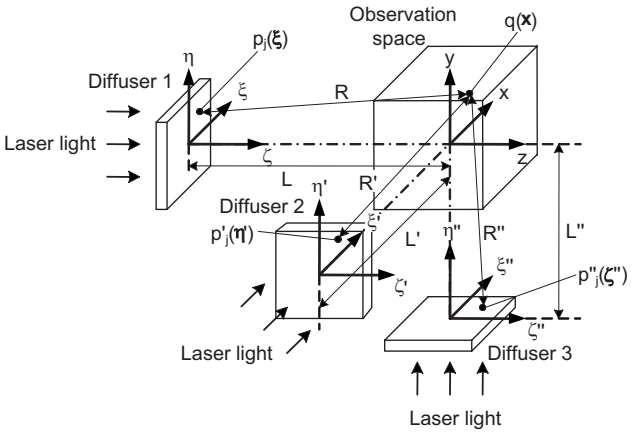

Fig. 1. Schematic diagram of the theoretical model to analyze superposed speckle fields.

D_1 and D_2. In this case the two speckle fields produced by D_1 and D_2 are added on an amplitude basis. The complex amplitude of scattered light from D_1 in the observation space is represented as

$$A_1(\mathbf{x}) = \sum_{j=1}^{N} \frac{1}{\sqrt{N}} a_{p_j q} \exp(i\phi_{p_j q}), \tag{1}$$

where $N^{-1/2}a_{p_j q}$ and $\phi_{p_j q}$ are the amplitude and the phase, respectively, of a wavelet propagating from scattering point $p_j(\boldsymbol{\xi})$ to observation point $q(\mathbf{x})$ with $\boldsymbol{\xi}=(\xi,\eta,0)$ and $\mathbf{x}=(x,y,z)$, and N is the number of scattering points. The scattered light from D_2 is also written as

$$A_2(\mathbf{x}) = \sum_{j=1}^{N'} \frac{1}{\sqrt{N'}} a_{p'_j q} \exp(i\phi_{p'_j q}), \tag{2}$$

where $N'^{-1/2}a_{p'_j q}$ and $\phi_{p'_j q}$ are the amplitude and the phase of a wavelet from scattering point $p'_j(\boldsymbol{\eta}')$ to $q(\mathbf{x})$ with $\boldsymbol{\eta}'=(0,\eta',\zeta')$, and N' is the number of scattering points on D_2. The total amplitude of the superposed field is given by

$$A(\mathbf{x}) = A_1(\mathbf{x}) + A_2(\mathbf{x}). \tag{3}$$

First, we consider the probability density function of the intensity of the resultant field. We assume that the field amplitudes $A_1(\mathbf{x})$ and $A_2(\mathbf{x})$ obey circular complex Gaussian statistics. In addition, if $a_{p_j q}$, $a_{p'_j q}$, $\phi_{p_j q}$, and $\phi_{p'_j q}$ are independent of one another and of the amplitudes and phases of all other wavelets, the amplitude of the total field also obeys circular complex Gaussian statistics. Therefore, the probability density function of intensity I becomes

$$p_I(I) = \frac{1}{\langle I\rangle} e^{-I/\langle I\rangle}, \tag{4}$$

where $\langle\cdots\rangle$ denotes the ensemble average. The density function is the same as that of single speckle fields, A_1 and A_2.

To characterize the structure of a superposed speckle distribution, the autocorrelation function of speckle intensity needs to be derived. For circular complex Gaussian fields, the correlation function is given by

$$\langle I(\mathbf{x}_1)I(\mathbf{x}_2)\rangle = \langle I(\mathbf{x}_1)\rangle\langle I(\mathbf{x}_2)\rangle[1 + |\gamma_A(\mathbf{x}_1,\mathbf{x}_2)|^2], \tag{5}$$

where

$$\langle I(\mathbf{x}_1)\rangle = \langle A(\mathbf{x}_1)A^*(\mathbf{x}_1)\rangle, \tag{6}$$

$$\langle I(\mathbf{x}_2)\rangle = \langle A(\mathbf{x}_2)A^*(\mathbf{x}_2)\rangle, \tag{7}$$

and $*$ denotes the complex conjugate. Here $\gamma_A(\mathbf{x}_1,\mathbf{x}_2)$ stands for the complex correlation coefficient of amplitude, which is defined as

$$\gamma_A(\mathbf{x}_1,\mathbf{x}_2) = \frac{\langle A(\mathbf{x}_1)A^*(\mathbf{x}_2)\rangle}{[\langle I(\mathbf{x}_1)\rangle\langle I(\mathbf{x}_2)\rangle]^{1/2}}. \tag{8}$$

The autocorrelation function of the total amplitude is given by

$$\langle A(\mathbf{x}_1)A^*(\mathbf{x}_2)\rangle = \langle A_1(\mathbf{x}_1)A_1^*(\mathbf{x}_2)\rangle + \langle A_2(\mathbf{x}_1)A_2^*(\mathbf{x}_2)\rangle + \langle A_1(\mathbf{x}_1)A_2^*(\mathbf{x}_2)\rangle + \langle A_2(\mathbf{x}_1)A_1^*(\mathbf{x}_2)\rangle. \tag{9}$$

By applying the Huygens–Fresnel principle to the scattered fields from D_1 and D_2, the complex amplitudes are expressed as

$$A_1(\mathbf{x}) = \frac{1}{i\lambda}\int\int_{-\infty}^{\infty} a_1(\boldsymbol{\xi})\frac{\exp(i2\pi R/\lambda)}{R}\mathrm{d}\xi\mathrm{d}\eta, \tag{10}$$

$$A_2(\mathbf{x}) = \frac{1}{i\lambda}\int\int_{-\infty}^{\infty} a_2(\boldsymbol{\eta}')\frac{\exp(i2\pi R'/\lambda)}{R'}\mathrm{d}\eta'\mathrm{d}\zeta', \tag{11}$$

where λ is the wavelength of incident light and $a_1(\boldsymbol{\xi})$ and $a_2(\boldsymbol{\eta}')$ represent the complex amplitudes just behind diffusers D_1 and D_2, respectively; R and R' are the distances from points $p_j(\boldsymbol{\xi})$ and $p'_j(\boldsymbol{\eta}')$ to $q(\mathbf{x})$, respectively:

$$R = |\mathbf{x}-\boldsymbol{\xi}| = [(x-\xi)^2 + (y-\eta)^2 + (z+L)^2]^{1/2}, \tag{12}$$

$$R' = |\mathbf{x}-\boldsymbol{\eta}'| = [(x+L')^2 + (y-\eta')^2 + (z-\zeta')^2]^{1/2}. \tag{13}$$

If we assume that $|x-\xi|$, $|y-\eta|$, and $|z|$ are much smaller than L and that $|x|$, $|y-\eta'|$, and $|z-\zeta'|$ are much smaller than L', R and R' are approximated as

$$R = z + L + \frac{(x-\xi)^2 + (y-\eta)^2}{2(z+L)}, \tag{14}$$

$$R' = x + L' + \frac{(y-\eta')^2 + (z-\zeta')^2}{2(x+L')}. \tag{15}$$

Substitution of Eqs. (14) and (15) into Eqs. (10) and (11) results in

$$A_1(\mathbf{x}) = \frac{1}{i\lambda L}\exp\left[i\frac{2\pi}{\lambda}(z+L)\right] \times \int\int_{-\infty}^{\infty} a_1(\boldsymbol{\xi})\exp\left\{i\frac{\pi[(x-\xi)^2 + (y-\eta)^2]}{\lambda(z+L)}\right\}\mathrm{d}\xi\mathrm{d}\eta, \tag{16}$$

$$A_2(\mathbf{x}) = \frac{1}{i\lambda L'} \exp\left[i\frac{2\pi}{\lambda}(x + L') \right] \times \int\int_{-\infty}^{\infty} a_2(\boldsymbol{\eta}') \exp\left\{ i\frac{\pi[(y-\eta')^2 + (z-\zeta')^2]}{\lambda(x+L')} \right\} \mathrm{d}\eta' \mathrm{d}\zeta', \tag{17}$$

where the denominators of the integrands in Eqs. (10) and (11) have been replaced with L and L', respectively.

To evaluate Eqs. (16) and (17), we have to specify the correlation functions of the field amplitudes $a_1(\boldsymbol{\xi})$ and $a_2(\boldsymbol{\eta}')$. Here we employ assumptions that the correlation area of each field is sufficiently small and that there is no correlation between the two fields, in which case

$$\langle a_1(\boldsymbol{\xi}_1) a_1^*(\boldsymbol{\xi}_2) \rangle = \kappa P(\boldsymbol{\xi}_1) P^*(\boldsymbol{\xi}_2) \delta(\boldsymbol{\xi}_1 - \boldsymbol{\xi}_2), \tag{18}$$

$$\langle a_2(\boldsymbol{\eta}_1') a_2^*(\boldsymbol{\eta}_2') \rangle = \kappa' P'(\boldsymbol{\eta}_1') P'^*(\boldsymbol{\eta}_2') \delta(\boldsymbol{\eta}_1' - \boldsymbol{\eta}_2'), \tag{19}$$

$$\langle a_1(\boldsymbol{\xi}_1) a_2^*(\boldsymbol{\eta}_2') \rangle = 0, \tag{20}$$

$$\langle a_2(\boldsymbol{\eta}_1') a_1^*(\boldsymbol{\xi}_2) \rangle = 0, \tag{21}$$

where κ and κ' are proportionality constants, functions $P(\boldsymbol{\xi})$ and $P'(\boldsymbol{\eta}')$ represent the amplitudes of the fields incident on D_1 and D_2, respectively, and $\delta(\boldsymbol{\xi}_1 - \boldsymbol{\xi}_2)$ and $\delta(\boldsymbol{\eta}_1' - \boldsymbol{\eta}_2')$ are two-dimensional delta functions. Under these assumptions, each term in Eq. (9) can be calculated as

$$\langle A_1(\mathbf{x}_1) A_1^*(\mathbf{x}_2) \rangle = c \exp\left(i\frac{2\pi}{\lambda}\Delta z \right) \left[i\frac{\pi}{\lambda}\left(\frac{x_1^2 + y_1^2}{z_1 + L} - \frac{x_2^2 + y_2^2}{z_2 + L} \right) \right] \times \int\int_{-\infty}^{\infty} |P(\boldsymbol{\xi})|^2 \times \exp\left[-i\frac{\pi}{\lambda}\frac{\Delta z}{(z_1 + L)(z_2 + L)}(\xi^2 + \eta^2) \right] \times \exp\left[-i\frac{2\pi}{\lambda}(\Delta x' \xi + \Delta y' \eta) \right] \mathrm{d}\xi \mathrm{d}\eta, \tag{22}$$

$$\langle A_2(\mathbf{x}_1) A_2^*(\mathbf{x}_2) \rangle = c' \exp\left(i\frac{2\pi}{\lambda}\Delta x \right) \left[i\frac{\pi}{\lambda}\left(\frac{y_1^2 + z_1^2}{x_1 + L'} - \frac{y_2^2 + z_2^2}{x_2 + L'} \right) \right] \times \int\int_{-\infty}^{\infty} |P'(\boldsymbol{\eta}')|^2 \times \exp\left[-i\frac{\pi}{\lambda}\frac{\Delta x}{(x_1 + L')(x_2 + L')}(\eta'^2 + \zeta'^2) \right] \times \exp\left[-i\frac{2\pi}{\lambda}(\Delta y'' \eta' + \Delta z' \zeta') \right] \mathrm{d}\eta' \mathrm{d}\zeta', \tag{23}$$

$$\langle A_1(\mathbf{x}_1) A_2^*(\mathbf{x}_2) \rangle = 0, \tag{24}$$

$$\langle A_2(\mathbf{x}_1) A_1^*(\mathbf{x}_2) \rangle = 0, \tag{25}$$

where

$$c = \frac{\kappa}{\lambda^2 L^2}, \qquad c' = \frac{\kappa'}{\lambda^2 L'^2}, \tag{26}$$

$$\Delta x = x_1 - x_2, \qquad \Delta z = z_1 - z_2, \tag{27}$$

$$\Delta x' = \frac{x_1}{z_1 + L} - \frac{x_2}{z_2 + L}, \qquad \Delta y' = \frac{y_1}{z_1 + L} - \frac{y_2}{z_2 + L},$$

$$\Delta z' = \frac{z_1}{x_1 + L'} - \frac{z_2}{x_2 + L'}, \tag{28}$$

$$\Delta y'' = \frac{y_1}{x_1 + L'} - \frac{y_2}{x_2 + L'}. \tag{29}$$

The average intensities at $\mathbf{x}_1$ and $\mathbf{x}_2$ then become

$$\langle I(\mathbf{x}_1) \rangle = \langle I(\mathbf{x}_2) \rangle \equiv \langle I_1 \rangle + \langle I_2 \rangle, \tag{30}$$

where

$$\langle I_1 \rangle = c \int\int_{-\infty}^{\infty} |P(\boldsymbol{\xi})|^2 \mathrm{d}\xi \mathrm{d}\eta, \tag{31}$$

$$\langle I_2 \rangle = c' \int\int_{-\infty}^{\infty} |P'(\boldsymbol{\eta}')|^2 \mathrm{d}\eta' \mathrm{d}\zeta'. \tag{32}$$

By substituting Eqs. (9), (24), (25), and (30), into Eq. (8), we obtain

$$\gamma_A(\mathbf{x}_1, \mathbf{x}_2) = \frac{\langle A_1(\mathbf{x}_1) A_1^*(\mathbf{x}_2) \rangle + \langle A_2(\mathbf{x}_1) A_2^*(\mathbf{x}_2) \rangle}{\langle I_1 \rangle + \langle I_2 \rangle}. \tag{33}$$

Thus the correlation function of intensity, Eq. (5), is evaluated by using Eqs. (22), (23), and (30)–(33).

2. Incoherent Addition

If the polarization direction of the light beam incident on D_1 is changed to the x direction, the two speckle fields from D_1 and D_2 do not interfere and are added on an intensity basis. The theoretical development here also applies to the case in which the two light beams are mutually incoherent. The probability density function of speckle intensity, which is composed of a sum of N independent speckle patterns with the same average intensity, is expressed as [12]

$$p_I(I) = \frac{N^N I^{N-1}}{(N-1)! \langle I \rangle^N} \exp\left(-N\frac{I}{\langle I \rangle} \right). \tag{34}$$

In the present case, the density function can be obtained by substituting $N=2$ into Eq. (34):

$$p_I(I) = \frac{4I}{\langle I \rangle^2} \exp\left(-\frac{2I}{\langle I \rangle} \right). \tag{35}$$

Since the total speckle intensity is the sum of the speckle intensities arising from two orthogonal polarization components, the correlation function of the intensity is written as

$$\langle I(\mathbf{x}_1)I(\mathbf{x}_2)\rangle = \langle [I_x(\mathbf{x}_1)+I_y(\mathbf{x}_1)][I_x(\mathbf{x}_2)+I_y(\mathbf{x}_2)]\rangle$$
$$= \langle I_x(\mathbf{x}_1)I_x(\mathbf{x}_2)\rangle + \langle I_y(\mathbf{x}_1)I_y(\mathbf{x}_2)\rangle + \langle I_x(\mathbf{x}_1)I_y(\mathbf{x}_2)\rangle + \langle I_y(\mathbf{x}_1)I_x(\mathbf{x}_2)\rangle, \quad (36)$$

where $I_x(\mathbf{x})$ and $I_y(\mathbf{x})$ are the x and y polarization components of the total intensity, respectively. Using the fact that the two polarization components are independent of each other, the third and the fourth terms in Eq. (36) are given by

$$\langle I_x(\mathbf{x}_1)I_y(\mathbf{x}_2)\rangle = \langle I_x(\mathbf{x}_1)\rangle\langle I_y(\mathbf{x}_2)\rangle = \langle I_1(\mathbf{x}_1)\rangle\langle I_2(\mathbf{x}_2)\rangle, \quad (37)$$

$$\langle I_y(\mathbf{x}_1)I_x(\mathbf{x}_2)\rangle = \langle I_y(\mathbf{x}_1)\rangle\langle I_x(\mathbf{x}_2)\rangle = \langle I_2(\mathbf{x}_1)\rangle\langle I_1(\mathbf{x}_2)\rangle, \quad (38)$$

where the relations $I_x(\mathbf{x})=I_1(\mathbf{x})$ and $I_y(\mathbf{x})=I_2(\mathbf{x})$ have been used, with $I_1(\mathbf{x})=|A_1(\mathbf{x})|^2$ and $I_2(\mathbf{x})=|A_2(\mathbf{x})|^2$. The correlation function then takes the form

$$\langle I(\mathbf{x}_1)I(\mathbf{x}_2)\rangle = \langle I_1(\mathbf{x}_1)\rangle\langle I_1(\mathbf{x}_2)\rangle + |\langle A_1(\mathbf{x}_1)A_1^*(\mathbf{x}_2)\rangle|^2 + \langle I_2(\mathbf{x}_1)\rangle\langle I_2(\mathbf{x}_2)\rangle + |\langle A_2(\mathbf{x}_1)A_2^*(\mathbf{x}_2)\rangle|^2 + \langle I_1(\mathbf{x}_1)\rangle\langle I_2(\mathbf{x}_2)\rangle + \langle I_2(\mathbf{x}_1)\rangle\langle I_1(\mathbf{x}_2)\rangle. \quad (39)$$

Assumption of the white-noise approximation given by Eqs. (18)–(21) results in

$$\langle I(\mathbf{x}_1)I(\mathbf{x}_2)\rangle = \langle I_1\rangle^2[1+|\gamma_{A_1}(\mathbf{x}_1,\mathbf{x}_2)|^2] + \langle I_2\rangle^2[1+|\gamma_{A_2}(\mathbf{x}_1,\mathbf{x}_2)|^2] + 2\langle I_1\rangle\langle I_2\rangle, \quad (40)$$

where $\langle I_1\rangle=\langle I_1(\mathbf{x}_1)\rangle=\langle I_1(\mathbf{x}_2)\rangle$ and $\langle I_2\rangle=\langle I_2(\mathbf{x}_1)\rangle=\langle I_2(\mathbf{x}_2)\rangle$. Here $\gamma_{A_1}(\mathbf{x}_1,\mathbf{x}_2)$ and $\gamma_{A_2}(\mathbf{x}_1,\mathbf{x}_2)$ are the complex correlation coefficients of amplitudes A_1 and A_2, respectively, which are given by

$$\gamma_{A_1}(\mathbf{x}_1,\mathbf{x}_2) = \frac{\langle A_1(\mathbf{x}_1)A_1^*(\mathbf{x}_2)\rangle}{[\langle I_1(\mathbf{x}_1)\rangle\langle I_1(\mathbf{x}_2)\rangle]^{1/2}} = \frac{\langle A_1(\mathbf{x}_1)A_1^*(\mathbf{x}_2)\rangle}{\langle I_1\rangle}, \quad (41)$$

$$\gamma_{A_2}(\mathbf{x}_1,\mathbf{x}_2) = \frac{\langle A_2(\mathbf{x}_1)A_2^*(\mathbf{x}_2)\rangle}{[\langle I_2(\mathbf{x}_1)\rangle\langle I_2(\mathbf{x}_2)\rangle]^{1/2}} = \frac{\langle A_2(\mathbf{x}_1)A_2^*(\mathbf{x}_2)\rangle}{\langle I_2\rangle}. \quad (42)$$

Equations (40)–(42) are evaluated by using Eqs. (22), (23), (31), and (32).

For the special case of $\langle I_1\rangle=\langle I_2\rangle=\langle I\rangle/2$, Eq. (40) further reduces to

$$\langle I(\mathbf{x}_1)I(\mathbf{x}_2)\rangle = \frac{\langle I\rangle^2}{4}[4+|\gamma_{A_1}(\mathbf{x}_1,\mathbf{x}_2)|^2+|\gamma_{A_2}(\mathbf{x}_1,\mathbf{x}_2)|^2]. \quad (43)$$

B. Superposition of Three Waves

1. Partially Coherent Addition

Next we consider the triple-wave configuration. In general, three speckle waves crossed orthogonally do not completely interfere because the direction of one polarization component of a wave coincides with the propagating direction of one of the other waves. To realize an interference of the speckle waves while keeping the equivalent polarization state in the x, y, and z directions, we analyze the case where diffusers D_1, D_2, and D_3 are illuminated with linearly polarized light beams with the polarization direction cosines of $(1/\sqrt{2}, 1/\sqrt{2}, 0)$, $(0, 1/\sqrt{2}, 1/\sqrt{2})$, and $(1/\sqrt{2}, 0, 1/\sqrt{2})$, respectively.

The complex amplitudes of scattered light from D_1, D_2, and D_3 are given, respectively, by Eqs. (1) and (2), and

$$A_3(\mathbf{x}) = \sum_{j=1}^{N''} \frac{1}{\sqrt{N''}} a_{p_j''q} \exp(i\phi_{p_j''q}), \quad (44)$$

where $N''^{-1/2}a_{p_j''q}$ and $\phi_{p_j''q}$ are the amplitude and the phase, respectively, of a wavelet from scattering point $p_j''(\boldsymbol{\zeta}'')$ to $q(\mathbf{x})$ with $\boldsymbol{\zeta}''=(\xi'',0,\zeta'')$, and N'' is the number of scattering points on D_3. The x, y, and z polarization components of the resulting field are related to the complex amplitudes of the three scattered fields arising from D_1, D_2, and D_3 as follows:

$$A_x(\mathbf{x}) = \frac{1}{\sqrt{2}}A_1(\mathbf{x}) + \frac{1}{\sqrt{2}}A_3(\mathbf{x}), \quad (45)$$

$$A_y(\mathbf{x}) = \frac{1}{\sqrt{2}}A_1(\mathbf{x}) + \frac{1}{\sqrt{2}}A_2(\mathbf{x}), \quad (46)$$

$$A_z(\mathbf{x}) = \frac{1}{\sqrt{2}}A_2(\mathbf{x}) + \frac{1}{\sqrt{2}}A_3(\mathbf{x}). \quad (47)$$

If the average intensities of the x, y, and z polarization components, $\langle I_x\rangle$, $\langle I_y\rangle$, and $\langle I_z\rangle$, respectively, are the same, all the complex correlation coefficients between different polarization components of the amplitude become 0.5. The probability density function of a sum of correlated speckle intensities can be obtained by calculating the eigenvalues of a coherency matrix defined by

$$[J] = \langle [A][A^\dagger]\rangle = \left\langle \begin{bmatrix} A_x \\ A_y \\ A_z \end{bmatrix} [A_x^* \quad A_y^* \quad A_z^*] \right\rangle = \begin{bmatrix} \langle I_x\rangle & \sqrt{\langle I_x\rangle\langle I_y\rangle}\gamma_{xy} & \sqrt{\langle I_x\rangle\langle I_z\rangle}\gamma_{xz} \\ \sqrt{\langle I_x\rangle\langle I_y\rangle}\gamma_{xy}^* & \langle I_y\rangle & \sqrt{\langle I_y\rangle\langle I_z\rangle}\gamma_{yz} \\ \sqrt{\langle I_x\rangle\langle I_z\rangle}\gamma_{xz}^* & \sqrt{\langle I_y\rangle\langle I_z\rangle}\gamma_{yz}^* & \langle I_z\rangle \end{bmatrix}. \quad (48)$$

Substituting $\langle I_x\rangle=\langle I_y\rangle=\langle I_z\rangle=\langle I\rangle/3$ and $\gamma_{xy}=\gamma_{xz}=\gamma_{yz}=0.5$ into Eq. (48) and applying a unitary linear transformation that diagonalizes $[J]$, we find the eigenvalues as $\lambda_1=\lambda_2=\langle I\rangle/6$, $\lambda_3=2\langle I\rangle/3$. In this case, the probability density function of the intensity becomes

$$p_I(I) = \frac{I}{\lambda_1(\lambda_1-\lambda_3)}\exp\left(-\frac{I}{\lambda_1}\right) - \frac{\lambda_3}{(\lambda_1-\lambda_3)^2}\exp\left(-\frac{I}{\lambda_1}\right) + \frac{\lambda_3}{(\lambda_1-\lambda_3)^2}\exp\left(-\frac{I}{\lambda_3}\right)$$
$$= -\left(\frac{12I}{\langle I\rangle^2}+\frac{8}{3\langle I\rangle}\right)\exp\left(-\frac{6I}{\langle I\rangle}\right) + \frac{8}{3\langle I\rangle}\exp\left(-\frac{3I}{2\langle I\rangle}\right). \quad (49)$$

The autocorrelation function of intensity is expressed as

$$\begin{aligned}\langle I(\mathbf{x}_1)I(\mathbf{x}_2)\rangle &= \langle [I_x(\mathbf{x}_1)+I_y(\mathbf{x}_1)+I_z(\mathbf{x}_1)][I_x(\mathbf{x}_2)+I_y(\mathbf{x}_2)\\ &\quad + I_z(\mathbf{x}_2)]\rangle = \langle I_x(\mathbf{x}_1)I_x(\mathbf{x}_2)\rangle + \langle I_y(\mathbf{x}_1)I_y(\mathbf{x}_2)\rangle\\ &\quad + \langle I_z(\mathbf{x}_1)I_z(\mathbf{x}_2)\rangle + \langle I_x(\mathbf{x}_1)I_y(\mathbf{x}_2)\rangle + \langle I_x(\mathbf{x}_1)I_z(\mathbf{x}_2)\rangle\\ &\quad + \langle I_y(\mathbf{x}_1)I_x(\mathbf{x}_2)\rangle + \langle I_y(\mathbf{x}_1)I_z(\mathbf{x}_2)\rangle + \langle I_z(\mathbf{x}_1)I_x(\mathbf{x}_2)\rangle\\ &\quad + \langle I_z(\mathbf{x}_1)I_y(\mathbf{x}_2)\rangle, \end{aligned} \tag{50}$$

where $I_z(\mathbf{x})$ is the z polarization component of the total intensity. Equations (45)–(47) show that scattered waves are added on an amplitude basis to form the x, y, and z polarization components of the total speckle amplitude. Thus the three polarization components also obey circular complex Gaussian statistics. It follows that the complex Gaussian moment theorem can be invoked to write each term in Eq. (50) as, for example,

$$\langle I_x(\mathbf{x}_1)I_y(\mathbf{x}_2)\rangle = \langle I_x(\mathbf{x}_1)\rangle\langle I_y(\mathbf{x}_2)\rangle + |\langle A_x(\mathbf{x}_1)A_y^*(\mathbf{x}_2)\rangle|^2. \tag{51}$$

The assumption of the white-noise approximation given by Eqs. (18) and (19), and $\langle a_3(\boldsymbol{\zeta}_1'')a_3^*(\boldsymbol{\zeta}_2'')\rangle = \kappa'' P''(\boldsymbol{\zeta}_1'')P''^*(\boldsymbol{\zeta}_2'')\delta(\boldsymbol{\zeta}_1''-\boldsymbol{\zeta}_2'')$ with $P''(\boldsymbol{\zeta}'')$ the amplitude of the field incident on D_3 leads to $\langle I_x(\mathbf{x}_1)\rangle = \langle I_x(\mathbf{x}_2)\rangle = \langle I_x\rangle$, $\langle I_y(\mathbf{x}_1)\rangle = \langle I_y(\mathbf{x}_2)\rangle = \langle I_y\rangle$, and $\langle I_z(\mathbf{x}_1)\rangle = \langle I_z(\mathbf{x}_2)\rangle = \langle I_z\rangle$. Equation (50) is then rewritten as

$$\begin{aligned}\langle I(\mathbf{x}_1)I(\mathbf{x}_2)\rangle &= \langle I_x\rangle^2[1+|\gamma_{A_x}(\mathbf{x}_1,\mathbf{x}_2)|^2] + \langle I_y\rangle^2[1+|\gamma_{A_y}(\mathbf{x}_1,\mathbf{x}_2)|^2]\\ &\quad + \langle I_z\rangle^2[1+|\gamma_{A_z}(\mathbf{x}_1,\mathbf{x}_2)|^2]\\ &\quad + \tfrac{1}{2}\langle I_1\rangle^2[1+|\gamma_{A_1}(\mathbf{x}_1,\mathbf{x}_2)|^2]\\ &\quad + \tfrac{1}{2}\langle I_2\rangle^2[1+|\gamma_{A_2}(\mathbf{x}_1,\mathbf{x}_2)|^2]\\ &\quad + \tfrac{1}{2}\langle I_3\rangle^2[1+|\gamma_{A_3}(\mathbf{x}_1,\mathbf{x}_2)|^2] + \tfrac{3}{2}\langle I_1\rangle\langle I_2\rangle\\ &\quad + \tfrac{3}{2}\langle I_2\rangle\langle I_3\rangle + \tfrac{3}{2}\langle I_3\rangle\langle I_1\rangle, \end{aligned} \tag{52}$$

where

$$\langle I_x\rangle = \frac{\langle I_1\rangle+\langle I_3\rangle}{2}, \qquad \langle I_y\rangle = \frac{\langle I_1\rangle+\langle I_2\rangle}{2}, \qquad \langle I_z\rangle = \frac{\langle I_2\rangle+\langle I_3\rangle}{2}, \tag{53}$$

and we have used the fact that the amplitudes A_1, A_2, and A_3 are independent of one another. The correlation coefficients of A_x, A_y, and A_z take the same form as Eq. (33), which are given by

$$\gamma_{A_x}(\mathbf{x}_1,\mathbf{x}_3) = \frac{\langle A_1(\mathbf{x}_1)A_1^*(\mathbf{x}_2)\rangle + \langle A_3(\mathbf{x}_1)A_3^*(\mathbf{x}_2)\rangle}{\langle I_1\rangle+\langle I_3\rangle}, \tag{54}$$

$$\gamma_{A_y}(\mathbf{x}_1,\mathbf{x}_2) = \frac{\langle A_1(\mathbf{x}_1)A_1^*(\mathbf{x}_2)\rangle + \langle A_2(\mathbf{x}_1)A_2^*(\mathbf{x}_2)\rangle}{\langle I_1\rangle+\langle I_2\rangle}, \tag{55}$$

$$\gamma_{A_z}(\mathbf{x}_1,\mathbf{x}_2) = \frac{\langle A_2(\mathbf{x}_1)A_2^*(\mathbf{x}_2)\rangle + \langle A_3(\mathbf{x}_1)A_3^*(\mathbf{x}_2)\rangle}{\langle I_2\rangle+\langle I_3\rangle}. \tag{56}$$

Equations (52)–(56) can be evaluated using Eqs. (22), (23), (31), (32), (41), and (42) together with

$$\gamma_{A_3}(\mathbf{x}_1,\mathbf{x}_2) = \frac{\langle A_3(\mathbf{x}_1)A_3^*(\mathbf{x}_2)\rangle}{[\langle I_3(\mathbf{x}_1)\rangle\langle I_3(\mathbf{x}_2)\rangle]^{1/2}} = \frac{\langle A_3(\mathbf{x}_1)A_3^*(\mathbf{x}_2)\rangle}{\langle I_3\rangle}, \tag{57}$$

$$\begin{aligned}\langle A_3(\mathbf{x}_1)A_3^*(\mathbf{x}_2)\rangle &= c''\exp\left(i\frac{2\pi}{\lambda}\Delta y\right)\left[i\frac{\pi}{\lambda}\left(\frac{z_1^2+x_1^2}{y_1+L''}-\frac{z_2^2+x_2^2}{y_2+L''}\right)\right]\\ &\quad\times\int\int_{-\infty}^{\infty}|P''(\boldsymbol{\zeta}')|^2\\ &\quad\times\exp\left[-i\frac{\pi}{\lambda}\frac{\Delta y}{(y_1+L'')(y_2+L'')}(\zeta''^2+\xi''^2)\right]\\ &\quad\times\exp\left[-i\frac{2\pi}{\lambda}(\Delta z''\zeta''+\Delta x''\xi'')\right]\mathrm{d}\zeta''\mathrm{d}\xi'', \end{aligned} \tag{58}$$

and

$$\langle I_3\rangle = c''\int\int_{-\infty}^{\infty}|P''(\boldsymbol{\zeta}')|^2\mathrm{d}\zeta''\mathrm{d}\xi'', \tag{59}$$

where

$$c'' = \frac{\kappa''}{\lambda^2 L''^2}, \tag{60}$$

$$\Delta y = y_1 - y_2, \tag{61}$$

$$\Delta x'' = \frac{x_1}{y_1+L''}-\frac{x_2}{y_2+L''}, \qquad \Delta z'' = \frac{z_1}{y_1+L''}-\frac{z_2}{y_2+L''}. \tag{62}$$

When $\langle I_1\rangle = \langle I_2\rangle = \langle I_3\rangle = \langle I\rangle/3$ is satisfied, Eq. (52) reduces to

$$\begin{aligned}\langle I(\mathbf{x}_1)I(\mathbf{x}_2)\rangle &= \frac{\langle I\rangle^2}{9}\Bigg[9+|\gamma_{A_x}(\mathbf{x}_1,\mathbf{x}_2)|^2+|\gamma_{A_y}(\mathbf{x}_1,\mathbf{x}_2)|^2\\ &\quad+|\gamma_{A_z}(\mathbf{x}_1,\mathbf{x}_2)|^2+\frac{1}{2}|\gamma_{A_1}(\mathbf{x}_1,\mathbf{x}_2)|^2\\ &\quad+\frac{1}{2}|\gamma_{A_2}(\mathbf{x}_1,\mathbf{x}_2)|^2+\frac{1}{2}|\gamma_{A_3}(\mathbf{x}_1,\mathbf{x}_2)|^2\Bigg]. \end{aligned} \tag{63}$$

2. Incoherent Addition

As a natural extension of the geometry discussed in Subsection 2.A.2, we consider the situation where the light beams incident on D_1, D_2, and D_3 are polarized in the x, y, and z directions, respectively.

If the average intensities of the three speckle waves are the same, the probability density function of the total intensity is given by substituting $N=3$ into Eq. (34):

$$p_I(I) = \frac{27I^2}{2\langle I\rangle^3}\exp\left(-\frac{3I}{\langle I\rangle}\right). \tag{64}$$

The autocorrelation function of intensity for the triple-wave configuration is expressed as Eq. (50). In the case of incoherent addition, all the cross terms in Eq. (50) can be factorized, resulting in

$$\begin{aligned}\langle I(\mathbf{x}_1)I(\mathbf{x}_2)\rangle &= \langle I_1(\mathbf{x}_1)\rangle\langle I_1(\mathbf{x}_2)\rangle + |\langle A_1(\mathbf{x}_1)A_1^*(\mathbf{x}_2)\rangle|^2 \\ &+ \langle I_2(\mathbf{x}_1)\rangle\langle I_2(\mathbf{x}_2)\rangle + |\langle A_2(\mathbf{x}_1)A_2^*(\mathbf{x}_2)\rangle|^2 \\ &+ \langle I_3(\mathbf{x}_1)\rangle\langle I_3(\mathbf{x}_2)\rangle + |\langle A_3(\mathbf{x}_1)A_3^*(\mathbf{x}_2)\rangle|^2 \\ &+ \langle I_1(\mathbf{x}_1)\rangle\langle I_2(\mathbf{x}_2)\rangle + \langle I_2(\mathbf{x}_1)\rangle\langle I_1(\mathbf{x}_2)\rangle \\ &+ \langle I_2(\mathbf{x}_1)\rangle\langle I_3(\mathbf{x}_2)\rangle + \langle I_3(\mathbf{x}_1)\rangle\langle I_2(\mathbf{x}_2)\rangle \\ &+ \langle I_3(\mathbf{x}_1)\rangle\langle I_1(\mathbf{x}_2)\rangle + \langle I_1(\mathbf{x}_1)\rangle\langle I_3(\mathbf{x}_2)\rangle. \end{aligned}\tag{65}$$

Assuming the white-noise approximation, Eq. (65) further reduces to

$$\begin{aligned}\langle I(\mathbf{x}_1)I(\mathbf{x}_2)\rangle &= \langle I_1\rangle^2[1 + |\gamma_{A_1}(\mathbf{x}_1,\mathbf{x}_2)|^2] + \langle I_2\rangle^2[1 + |\gamma_{A_2}(\mathbf{x}_1,\mathbf{x}_2)|^2] \\ &+ \langle I_3\rangle^2[1 + |\gamma_{A_3}(\mathbf{x}_1,\mathbf{x}_2)|^2] + 2\langle I_1\rangle\langle I_2\rangle + 2\langle I_2\rangle\langle I_3\rangle \\ &+ 2\langle I_3\rangle\langle I_1\rangle. \end{aligned}\tag{66}$$

For the special case of $\langle I_1\rangle=\langle I_2\rangle=\langle I_3\rangle=\langle I\rangle/3$, Eq. (66) becomes

$$\begin{aligned}\langle I(\mathbf{x}_1)I(\mathbf{x}_2)\rangle &= \frac{\langle I\rangle^2}{9}[9 + |\gamma_{A_1}(\mathbf{x}_1,\mathbf{x}_2)|^2 + |\gamma_{A_2}(\mathbf{x}_1,\mathbf{x}_2)|^2 \\ &+ |\gamma_{A_3}(\mathbf{x}_1,\mathbf{x}_2)|^2]. \end{aligned}\tag{67}$$

3. THEORETICAL RESULTS

A. Probability Density Function

First, we present the results of the first-order statistics of superposed speckles arising from two or three scattered waves crossed orthogonally. Figure 2 shows the probability density functions for the four different situations analyzed in a previous section. For the case in which two fully developed speckle waves completely interfere with each other, the resulting speckle is also fully developed, and its intensity distribution follows the negative exponential density function [dashed curve in Fig. 2(a)]. Incoherent addition of two or three speckle waves reduces the ratio of dark regions in the speckles, making the density function concentrated around a particular intensity value that lies between zero and the average intensity (solid curves in Fig. 2). The intensity at which the density function takes the maximum approaches the average intensity as the number of speckle waves increases. It should be noted that, for the three partially interfering speckle waves we analyzed, the shape of the probability density function [dashed curve in Fig. 2(b)] is similar to the one with incoherent addition, except that the peak position is shifted toward zero intensity.

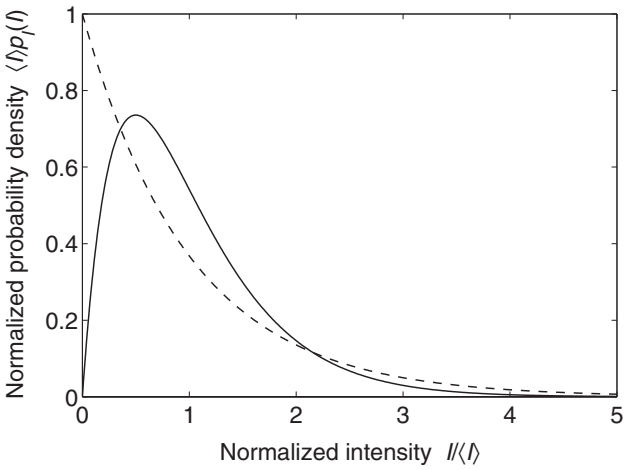

(a)

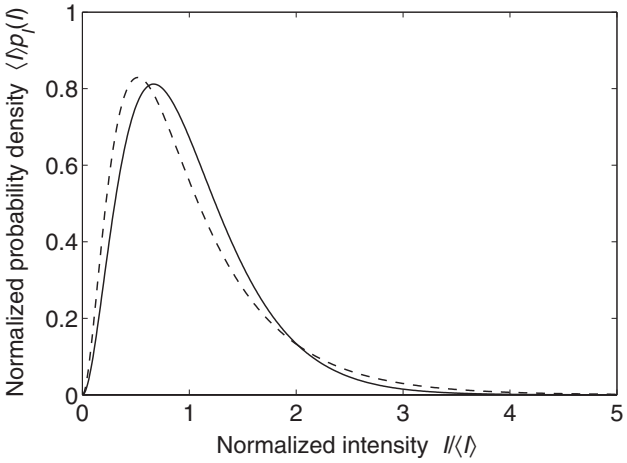

(b)

Fig. 2. Probability density functions for (a) two and (b) three speckle waves. The solid curves denote the case of incoherent addition, while the dashed curves represent (a) coherent addition and (b) partially coherent addition.

B. Correlation Function

To calculate the correlation function of the superposed speckle distributions, we must specify the intensity profiles of light incident on the diffusers. Two different intensity distributions of incident light are used for the following analysis. One is a commonly used Gaussian beam illumination:

$$\begin{aligned}|P(\boldsymbol{\xi})|^2 &= \exp[-2|\boldsymbol{\xi}|^2/w^2], \\ |P'(\boldsymbol{\eta}')|^2 &= \exp[-2|\boldsymbol{\eta}'|^2/w^2], \\ |P''(\boldsymbol{\zeta}'')|^2 &= \exp[-2|\boldsymbol{\zeta}''|^2/w^2], \end{aligned}\tag{68}$$

where w is the radius of the beam spot. The other is a power-law beam illumination:

$$|P(\boldsymbol{\xi})|^2 = |\boldsymbol{\xi}|^{-D}, \quad |P'(\boldsymbol{\eta}')|^2 = |\boldsymbol{\eta}'|^{-D}, \quad |P''(\boldsymbol{\zeta}'')|^2 = |\boldsymbol{\zeta}''|^{-D}, \tag{69}$$

which produces speckle with fractal properties [11]. For simplicity, we consider the cases of $\langle I_1\rangle=\langle I_2\rangle=\langle I\rangle/2$ for two waves and $\langle I_1\rangle=\langle I_2\rangle=\langle I_3\rangle=\langle I\rangle/3$ for three waves. In what follows, we will present the normalized autocorrelation function of intensity fluctuations $c_I(\mathbf{x}_1,\mathbf{x}_2)$ instead of

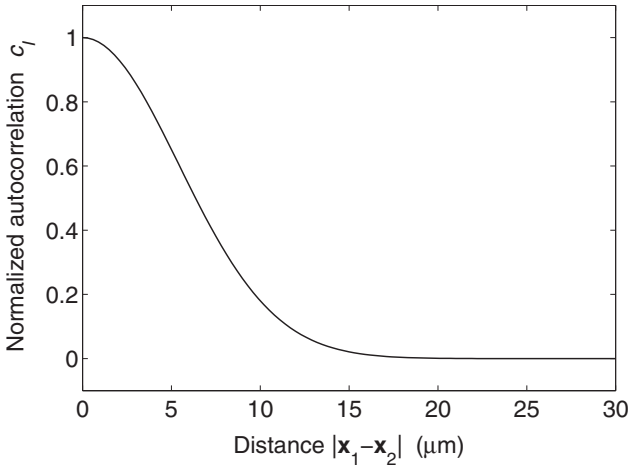

(a)

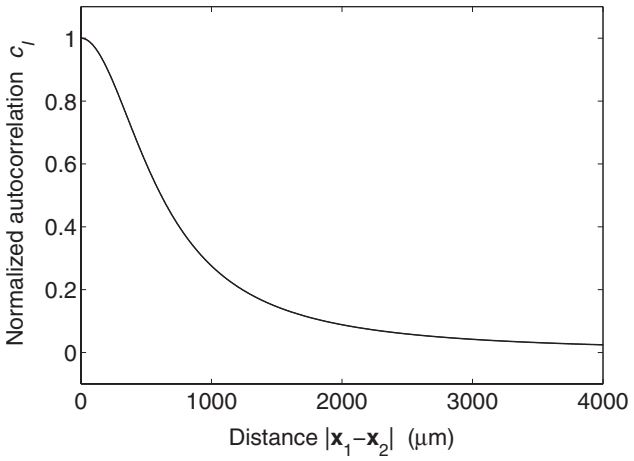

(b)

Fig. 3. Intensity correlation functions for a single speckle wave as a function of (a) Δx or Δy with $\Delta z=0$ and (b) Δz with $\Delta x'=\Delta y'=0$. The values of parameters are $\lambda=600$ nm, $w=2.5$ mm, $L=100$ mm, and $z_2=0$.

$\langle I(\mathbf{x}_1)I(\mathbf{x}_2)\rangle$. The correlation functions $c_I(\mathbf{x}_1,\mathbf{x}_2)$ for the speckles produced by (i) one scattered wave, (ii) coherent addition of two scattered waves, (iii) incoherent addition of two scattered waves, (iv) partially coherent addition of three scattered waves, and (v) incoherent addition of three scattered waves are considered, which are given, respectively, by

$$c_I(\mathbf{x}_1,\mathbf{x}_2)=|\gamma_{A_1}(\mathbf{x}_1,\mathbf{x}_2)|^2, \tag{70}$$

$$c_I(\mathbf{x}_1,\mathbf{x}_2)=|\gamma_A(\mathbf{x}_1,\mathbf{x}_2)|^2, \tag{71}$$

$$c_I(\mathbf{x}_1,\mathbf{x}_2)=\tfrac{1}{2}[|\gamma_{A_1}(\mathbf{x}_1,\mathbf{x}_2)|^2+|\gamma_{A_2}(\mathbf{x}_1,\mathbf{x}_2)|^2], \tag{72}$$

$$c_I(\mathbf{x}_1,\mathbf{x}_2)=\tfrac{2}{9}\Big[|\gamma_{A_x}(\mathbf{x}_1,\mathbf{x}_2)|^2+|\gamma_{A_y}(\mathbf{x}_1,\mathbf{x}_2)|^2+|\gamma_{A_z}(\mathbf{x}_1,\mathbf{x}_2)|^2+\tfrac{1}{2}|\gamma_{A_1}(\mathbf{x}_1,\mathbf{x}_2)|^2+\tfrac{1}{2}|\gamma_{A_2}(\mathbf{x}_1,\mathbf{x}_2)|^2+\tfrac{1}{2}|\gamma_{A_3}(\mathbf{x}_1,\mathbf{x}_2)|^2\Big], \tag{73}$$

$$c_I(\mathbf{x}_1,\mathbf{x}_2)=\tfrac{1}{3}[|\gamma_{A_1}(\mathbf{x}_1,\mathbf{x}_2)|^2+|\gamma_{A_2}(\mathbf{x}_1,\mathbf{x}_2)|^2+|\gamma_{A_3}(\mathbf{x}_1,\mathbf{x}_2)|^2]. \tag{74}$$

We also conducted a computer simulation in which speckle fields were generated numerically using a Huygens–Fresnel elementary wave calculation [13]. The simulation results visualize the intensity distribution of superposed speckles and help us understand their 3D structures.

1. Gaussian Beam Illumination

If a diffuser is illuminated with a single Gaussian beam, we have an ordinary speckle distribution, and its characteristics have already been studied. One of the most important features of the 3D speckle field is that the size of the speckle grain measured in the direction of the optical axis is much larger than that measured in the directions perpendicular to the optical axis. This anisotropic spatial distribution of speckles causes the intensity correlation function to be direction dependent.

In the plane perpendicular to the optical axis, i.e., $z_1=z_2=z_0$, the correlation function is given by

$$c_I(\mathbf{x}_1,\mathbf{x}_2)=\exp\left[-\frac{\pi^2w^2}{\lambda^2(z_0+L)^2}(\Delta x^2+\Delta y^2)\right], \tag{75}$$

where we have assumed that only D_1 is illuminated in Fig. 1. On the other hand, if $\mathbf{x}_1$ and $\mathbf{x}_2$ are on the z axis or,

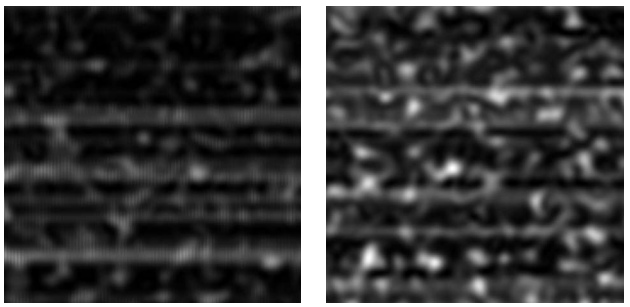

(a) (b)

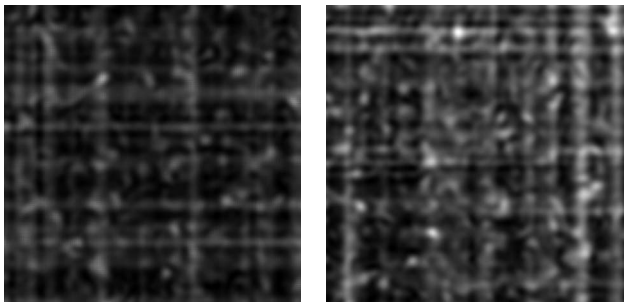

(c) (d)

Fig. 4. Intensity distributions in the xy plane with the area of 120×120 μm^2 for (a),(b) two speckle waves propagating in the x and z directions and (c),(d) three speckle waves propagating in the x, y, and z directions. Here (a) and (c) are for coherent addition, while (b) and (d) are for incoherent addition. The parameter values are $\lambda=600$ nm, $w=2.5$ mm, and $L=L'=L''=100$ mm. The horizontal axis is the x axis.

more generally, $\Delta x' = \Delta y' = 0$, the correlation function becomes

$$c_I(\mathbf{x}_1, \mathbf{x}_2) = \left| 1 + \left(\frac{w^2}{2} \right) \frac{i\pi\Delta z}{\lambda(z_2 + L)^2 + \lambda(z_2 + L)\Delta z} \right|^{-2}. \tag{76}$$

The 3D speckle distribution is nonstationary in the longitudinal direction.

Figure 3 shows the normalized correlation function of intensity fluctuations in the transverse and longitudinal directions. We can see that the width of the correlation function in the direction of the optical axis is by 2 orders of magnitude larger than that of the correlation of a speckle pattern observed in the transverse plane.

For the two-speckle-wave configuration, intensity distributions such as shown in Figs. 4(a) and 4(b) were obtained by our simulation. It is seen that elongated speckle grains are superposed on a normal speckle pattern. Coherent addition of two waves gives rise to a one-dimensional (1D) interference fringe pattern in 3D space. Although the period of the fringes is too small for each fringe to be resolved in Fig. 4(a), we can recognize many fine fringes in the vertical direction. There is no such periodic structure in Fig. 4(b), which is generated by an addition of two waves on an intensity basis.

The autocorrelation functions of intensity fluctuations for two scattered waves added coherently and incoherently are plotted in Fig. 5. In order to illustrate the direction dependence of the correlation function, we present two different correlation functions; one is plotted against $\Delta x = x_1 - x_2$ with $x_2 = y_1 = y_2 = z_1 = z_2 = 0$, and the other is plotted against $|\mathbf{x}_1 - \mathbf{x}_2|$ with $x_1 = y_1$ and $x_2 = y_2 = z_1 = z_2 = 0$; i.e., the two points lie on a straight line $y = x$. For the coherent addition we can see periodic modulations with the period of λ and $\sqrt{2}\lambda$ in the autocorrelation curves in Figs. 5(a) and 5(b), respectively. These modulations are getting smaller as the distance between the two points becomes larger and almost vanish when the distance is beyond the average speckle size. This indicates that the deterministic phase relation between the fringes is maintained only within each speckle grain.

Another interesting feature of orthogonally crossed speckle fields is that a long-range correlation exists in the direction of the optical axes. Since this is caused by the shape of elongated speckles, the correlation curves plotted in diagonal directions contain only a short-range correlation component. Because only $\langle A_2(\mathbf{x}_1) A_2^*(\mathbf{x}_2) \rangle$ contributes

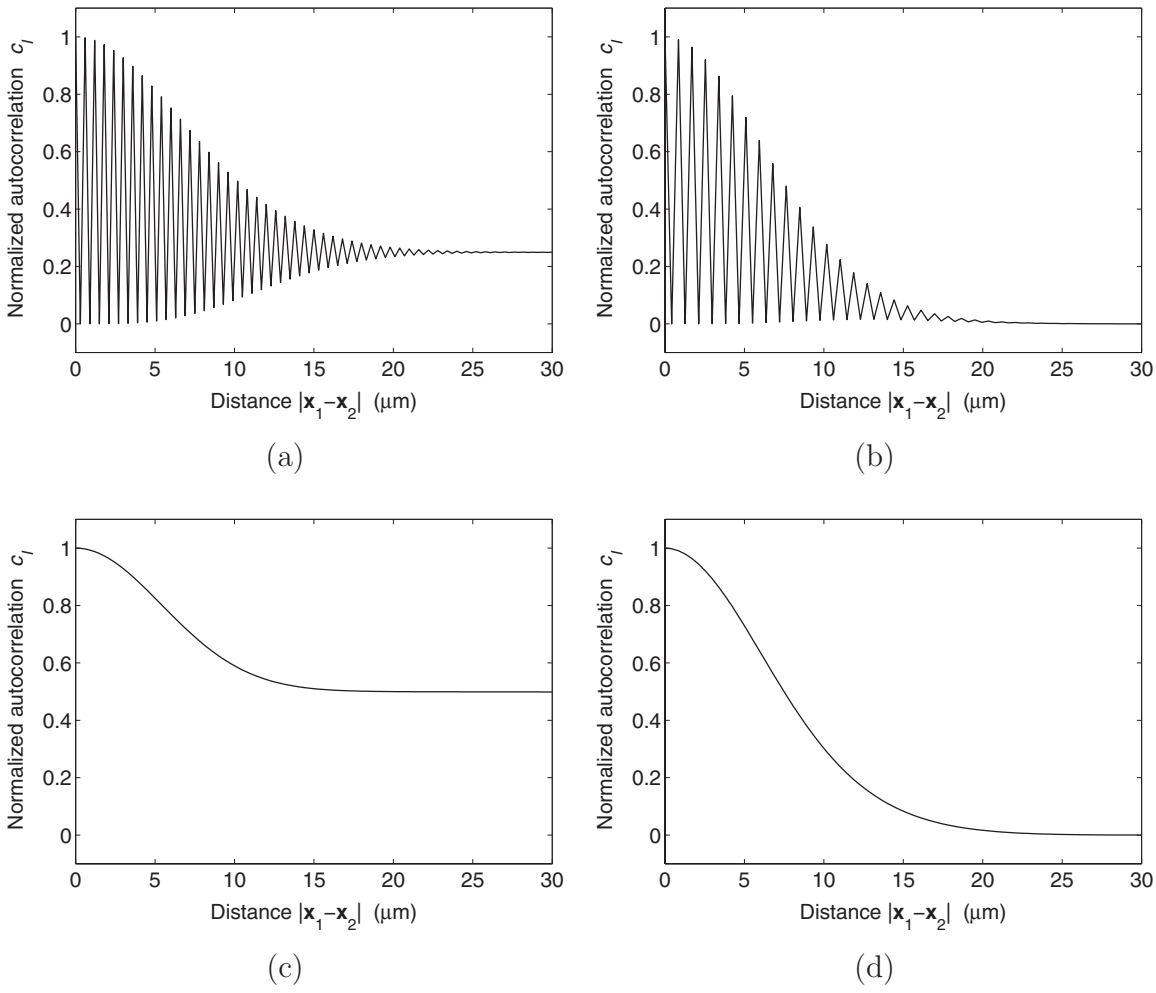

Fig. 5. Intensity correlation functions for (a),(b) coherent addition and (c),(d) incoherent addition of two speckle waves as a function of (a),(c) Δx with $x_2 = y_1 = y_2 = z_1 = z_2 = 0$ and (b),(d) $|\mathbf{x}_1 - \mathbf{x}_2|$ with $x_1 = y_1$ and $x_2 = y_2 = z_1 = z_2 = 0$. The parameter values are the same as those in Fig. 4.

to the long-range correlation in Figs. 5(a) and 5(c), the ratio of the long-range correlation component is 0.5 for the incoherent addition, while its value decreases to 0.25 for the coherent addition. As can be seen from a horizontal stripe pattern in Fig. 4(a), the long-range component survives even if two scattered waves interfere perfectly.

The intensity distributions for the three-speckle-wave configuration are shown in Figs. 4(c) and 4(d). The scattered wave propagating in the y direction is added to the speckle patterns shown in Figs. 4(a) and 4(b). Three scattered waves interfering with one another form a two-dimensional (2D) periodic structure in each speckle grain. Figure 6 shows the autocorrelation functions of intensity fluctuations for three scattered waves added partially coherently and incoherently. The horizontal axis variable is the same as that in Fig. 5. In Fig. 6(a), the modulation of the correlation function reduces because the partially correlated x, y, and z polarization components are added on an intensity basis. The ratio of the long-range correlation component for the partially coherent and coherent additions are 2/9 and 1/3, respectively.

2. Power-Law Beam Illumination

A fractal is a shape that has a fine structure at each scale and is self-similar, at least in a statistical sense. In terms of random lasers and optical amplifiers, it is possible to enhance optical gain and emissions using fractal structures [14,15]. It is therefore worthwhile to study superposed speckle waves with fractal properties. To generate a fractal speckle wave, we usually employ an illuminating beam with a power-law intensity distribution, $I(\rho) \sim \rho^{-D}$, with ρ the radial distance in the diffuser plane. The power-law beam illumination results in a fractal speckle pattern across a plane perpendicular to the optical axis.

The intensity correlation function of a fractal speckle pattern in the transverse plane is given by [11]

$$c_I(r) \propto r^{2(D-2)} \tag{77}$$

for $1<D<2$, where $r=(\Delta x^2+\Delta y^2)^{1/2}$. In Fig. 7(a), Eq. (77) is plotted for various power exponents D. Because the correlation obeys the power law, its value decreases linearly in a log–log plot. In general, the relationship between the dimension D_s of a fractal object and the correlation function $C(r)$ of its density is expressed as

$$C(r) \propto r^{-(d-D_s)}, \tag{78}$$

where r is the distance between two points and d is the Euclidean dimension of the space where the fractal object is embedded. In actual situations the scale range of frac-

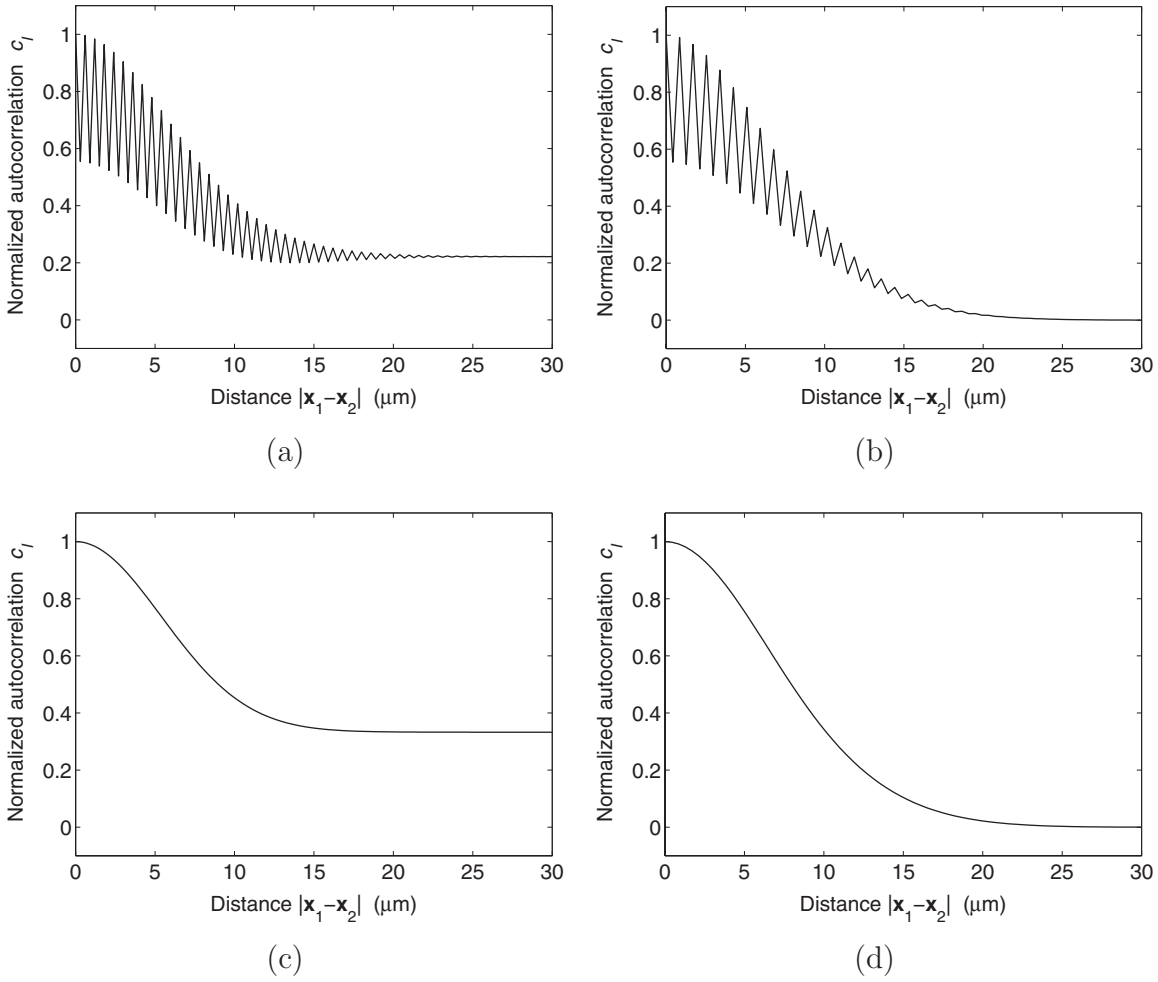

Fig. 6. Intensity correlation functions for (a),(b) partially coherent addition and (c),(d) incoherent addition of three speckle waves as a function of (a),(c) Δx with $x_2=y_1=y_2=z_1=z_2=0$ and (b),(d) $|\mathbf{x}_1-\mathbf{x}_2|$ with $x_1=y_1$ and $x_2=y_2=z_1=z_2=0$. The parameter values are the same as those in Fig. 4.

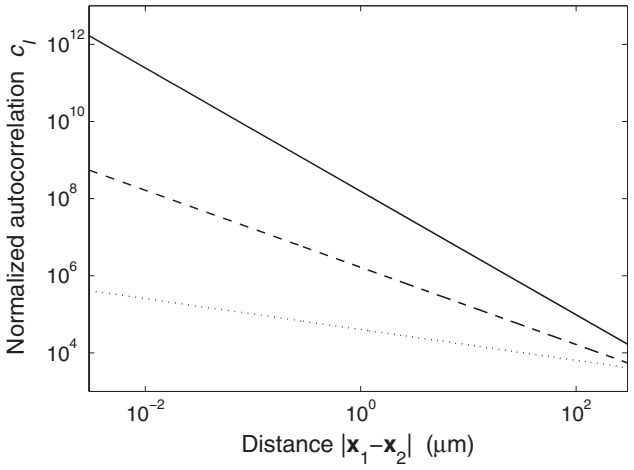

(a)

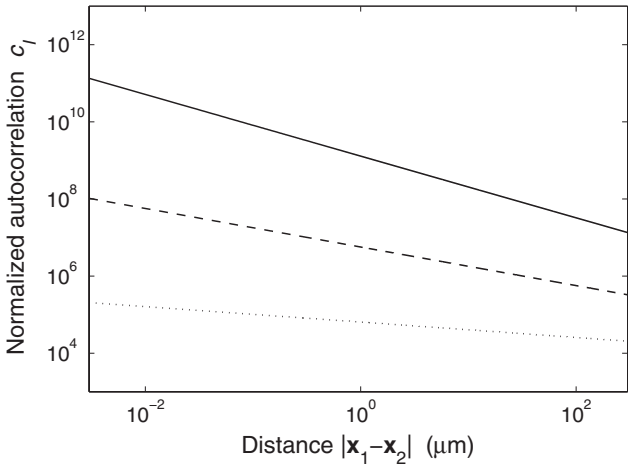

(b)

Fig. 7. Intensity correlation functions for a single fractal speckle wave as a function of (a) Δx or Δy with $\Delta z=0$ and (b) Δz with $\Delta x'=\Delta y'=0$ for $D=1.2$ (solid line), 1.5 (dashed line), and 1.8 (dotted line). The parameter values are $\lambda=600$ nm, $L=100$ mm, and $z_2=0$.

tality is limited; the function $C(r)$ has a finite value at $r=0$ and reaches another finite value when r exceeds the extent of fractality. It should be noted, therefore, that Eq. (78) holds in a limited range of r. Comparing Eqs. (77) and (78) gives the fractal dimension of $2D-2$ in 2D space.

On the other hand, the axial correlation function as a function of Δz is given by

$$c_I(\mathbf{x}_1,\mathbf{x}_2) \propto \left| \frac{(z_2+L)(z_2+\Delta z+L)}{\Delta z} \times \left(-\frac{i\Delta z}{\lambda(z_2+L)^2+\lambda(z_2+L)\Delta z} \right)^{D/2} \right|^2. \quad (79)$$

This function is found to follow asymptotically [16]

$$c_I(\mathbf{x}_1,\mathbf{x}_2) \propto \Delta z^{D-2} \quad (80)$$

for $\Delta z \ll L$. Figure 7(b) shows the correlation function of intensity fluctuations in the direction of the optical axis. The decay rate of the function is smaller than that for the transverse speckle pattern. The fractal dimension in the direction of the optical axis is found to be $D-1$ in 1D space.

Next we consider a superposition of two fractal speckle waves. Simulations were conducted under the same conditions as in the case of the Gaussian beam illumination. Figure 8 shows examples of the intensity distribution of crossed fractal speckle waves in the xy plane for $D=1.2$, 1.5, and 1.8. To avoid the singularity at the origin of a power function, we used $I(\rho)=\langle I(0)\rangle[1+(\alpha\rho)^2]^{-D/2}$ for incident light, with α being a parameter to determine the behavior of the function around the origin. Stripe patterns similar to the ones in Figs. 4(a) and 4(b) appear in the fractal speckles. The speckle size, however, seems much smaller than that of the Gaussian beam case; the reason for this difference is that the incident beam with the approximate power-law intensity distribution spreads

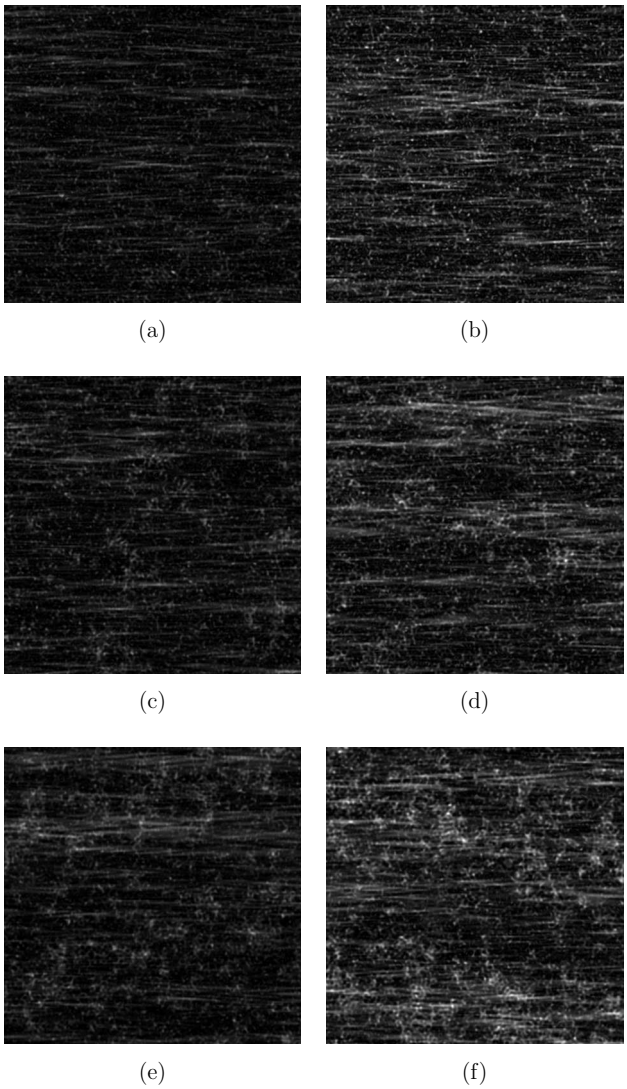

(a) (b) (c) (d) (e) (f)

Fig. 8. Intensity distributions of superposed fractal speckle waves propagating in the x and z directions for (a),(b) $D=1.2$; (c),(d) 1.5; and (e),(f) 1.8. The area of 120×120 μm^2 in the xy plane is shown. Here (a), (c), and (e) are for coherent addition, while (b), (d), and (f) are for incoherent addition. The parameter values are $\lambda=600$ nm and $L=L'=100$ mm. The horizontal axis is the x axis.

widely across the diffuser plane. At the same time, there are some large speckles that result from the central part of the power-law beam, the region where the illuminating intensity is very high. It is also seen that larger clusters and longer fibrous structures appear for larger power exponent D, which make the range of correlation larger.

The theoretical results for the autocorrelation function of intensity fluctuations arising from two crossed fractal speckle waves are shown in Fig. 9. It is seen from Fig. 9(a) that a periodic modulation exists in the correlation curves, reflecting the interference patterns shown in Figs. 8(a), 8(c), and 8(e) for coherent addition. There is no such modulation in the correlation functions in Fig. 9(b) for incoherent addition, and the correlation decreases almost linearly in a log–log plot, exhibiting fractal properties. However, each correlation function has two different power exponents, depending on the correlation range. In short ranges of $\Delta x < 0.1$ μm, the slope of the correlation function is $2(D-2)$, which coincides with the one for a fractal speckle pattern produced by a single laser beam [Fig. 7(a)]. As the correlation distance increases, the slope of the function approaches $D-2$, which is the slope of the axial correlation function of a single fractal speckle wave [Fig. 7(b)]. We can see this behavior in the case of coherent addition if the modulation of the correlation function is averaged out.

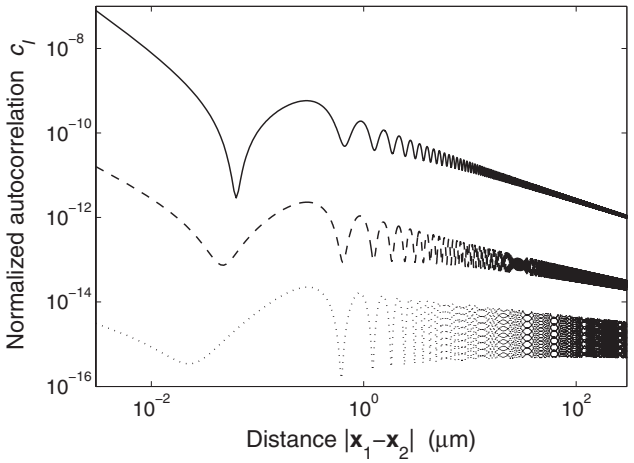

(a)

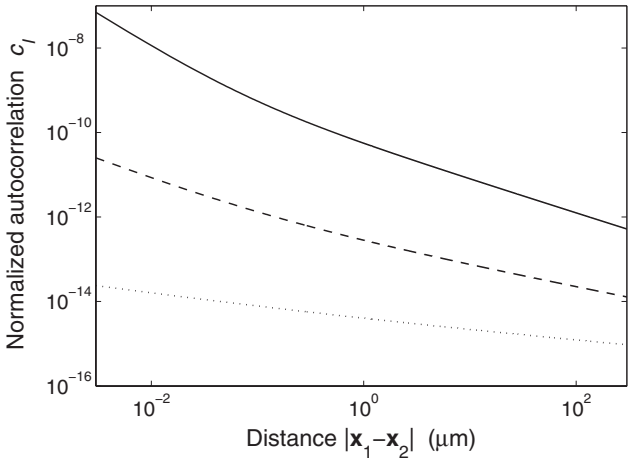

(b)

Fig. 9. Intensity correlation functions for (a) coherent addition and (b) incoherent addition of two fractal speckle waves as a function of Δx with $x_2=y_1=y_2=z_1=z_2=0$. The parameter values are the same as those in Fig. 8.

For the three-speckle-wave configuration, we have intensity distributions such as shown in Fig. 10. In this case, cross-stitch patterns appear in the xy, yz, and xz planes. Figure 11 shows the intensity correlation functions for partially coherent addition and incoherent addition of three fractal speckle waves. Although the degree of modulation for the correlation function in Fig. 11(a) is smaller than that for the two-wave case, the two correlation functions exhibit the same behavior. In the case of incoherent addition, we have almost the same correlation function as the one in Fig. 9(b).

As shown in Figs. 9 and 11, the intensity distribution formed with a superposition of two or three crossed frac-

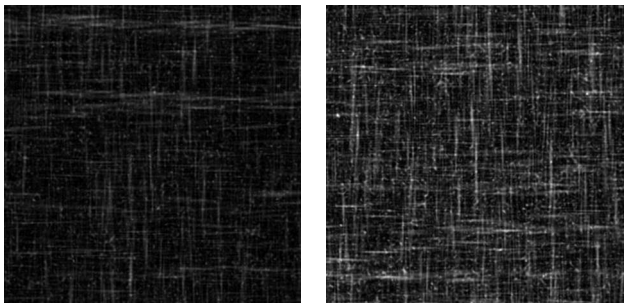

(a) (b)

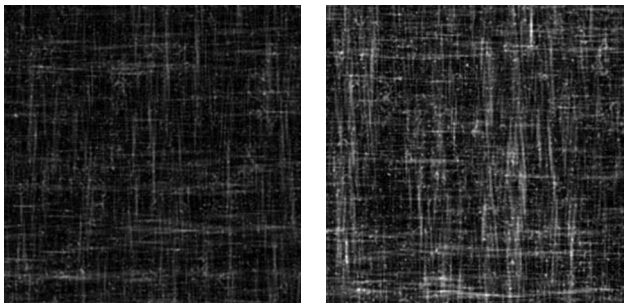

(c) (d)

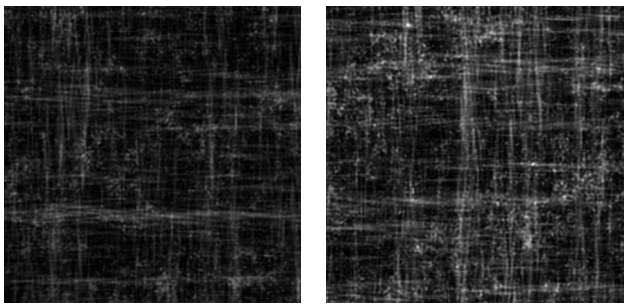

(e) (f)

Fig. 10. Intensity distributions of superposed fractal speckle waves propagating in the x, y, and z directions for (a),(b) $D=1.2$; (c),(d) 1.5; and (e),(f) 1.8. The area of 120×120 μm^2 in the xy plane is shown. Here (a), (c), and (e) are for coherent addition, while (b), (d), and (f) are for incoherent addition. The parameter values are $\lambda=600$ nm and $L=L'=L''=100$ mm. The horizontal axis is the x axis.

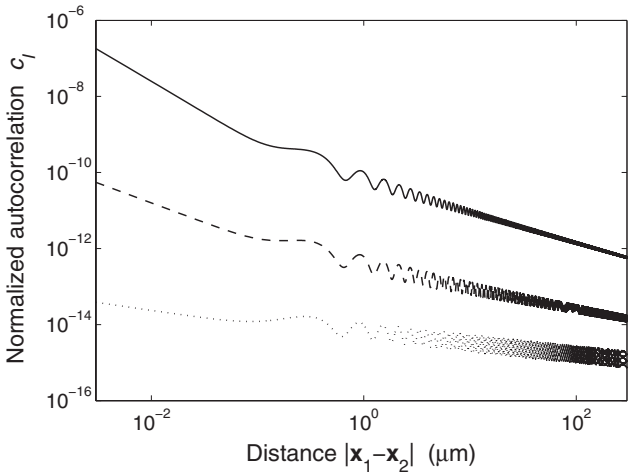

(a)

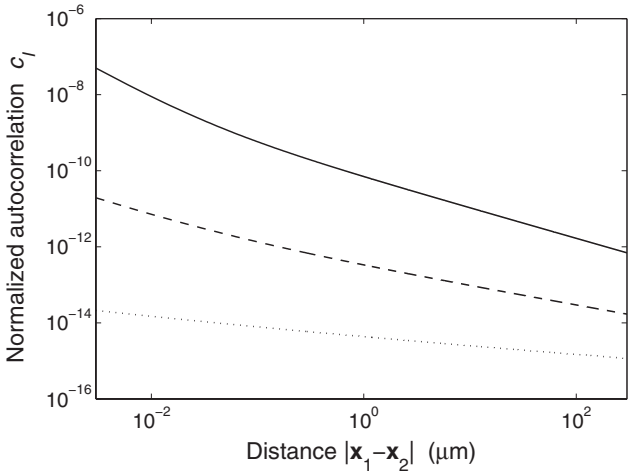

(b)

Fig. 11. Intensity correlation functions for (a) partially coherent addition and (b) incoherent addition of three fractal speckle waves as a function of Δx with $x_2=y_1=y_2=z_1=z_2=0$. The parameter values are the same as those in Fig. 10.

tal speckle waves exhibits different scaling laws in short ($\Delta x<0.1$ μm) and long ($\Delta x>1$ μm) correlation ranges. It should be noted, however, that the two-scaling property appears only in the axial directions. We found that, as the correlation direction is getting away from the axial directions, the two-scaling property disappears rapidly, and the power exponent of the correlation function in the long range eventually becomes the same as that in the short range. Therefore, the speckle pattern in the transverse plane is statistically isotropic in the short range but anisotropic in the long range. It follows that the superposed fractal speckle pattern is not self-similar in any mathematically rigorous sense. As a result, we cannot determine the fractal dimension of such a pattern uniquely. However, to simplify the present analysis, we introduce the fractal dimension in a particular direction, which is evaluated from the power exponent of the correlation function in that direction.

By applying Eq. (78) with $d=2$ to the theoretical results, the fractal dimension D_s of the superposed speckle pattern in the direction of the optical axes is evaluated to be 0.4, 1.0, and 1.6 in the short scale range and 1.2, 1.5, and 1.8 in the long scale range for $D=1.2$, 1.5, and 1.8, respectively. The dimension in the directions other than the optical axes is found to be 0.4, 1.0, and 1.6 in all scale ranges for $D=1.2$, 1.5, and 1.8, respectively. In our simulations, it was difficult to evaluate the correlation function in ranges less than 1 μm. Thus only the fractal dimension of the long scale range was evaluated numerically for the incoherent addition of three speckle waves. The dimensions were found to be 1.21, 1.58, and 1.68 in the x direction and 0.40, 0.95, and 1.57 in the ±45° directions with respect to the x axis for $D=1.2$, 1.5, and 1.8, respectively. The discrepancies between theory and simulation could be due to the fact that the number of data points used in our simulation is not large enough to reproduce speckle patterns that have scaling properties in a wide range.

4. CONCLUSION

We investigated the statistical properties of the intensity distribution of orthogonally crossed speckle waves. It was shown that the speckle distribution is anisotropic, and long-range correlation exists in the direction of the optical axes. In the case of the speckle waves interfering with one another, the intensity distribution is macroscopically random but microscopically periodic due to the interference of two or three speckle waves. The structure of superposed fractal speckles exhibits different scaling properties, depending on the correlation range. Two different scaling behaviors appear only in the axial directions, which makes the intensity distribution anisotropic even in the transverse plane.

These complex structures of the superposed speckles can be a subject of study for light scattering if their intensity distributions are preserved in photoresist or photopolymer. In particular, the spatial structure produced by coherent addition of scattered waves seems interesting, because it can be considered as an assemblage of photonic crystals that are distributed randomly but oriented in a certain direction. The combination of random and regular structures may find applications in the field of random lasers.

Random lasers need disordered media with gain instead of well-defined cavities and homogeneous active media [17]. Various kinds of materials have been used for providing light scattering and gain in random lasers; particle suspensions that contain dye solutions, polymers with scatterers and dyes, and semiconductor or rare-earth-doped powders are typical disordered media for observing random laser emissions. A random medium made by means of interference lithography serves as an alternative host medium for random lasers. Because of its periodicity, the fabricated media has a possibility of controlling the lasing modes, which is crucial to making random lasers more practical. The light scattering properties and the structural stability of the speckle random media need to be studied to elucidate its feasibility as a random laser medium or diffusers for various purposes.

ACKNOWLEDGMENTS

This work was supported by Grant-in-Aid for Scientific Research (C) from the Ministry of Education, Culture, Sports, Science, and Technology (MEXT).

REFERENCES

1. V. Berger, O. Gauthier-Lafaye, and E. Costard, "Photonic band gaps and holography," J. Appl. Phys. **82**, 60–64 (1997).
2. M. Campbell, D. N. Sharp, M. T. Harrison, R. G. Denning, and A. J. Turberfield, "Fabrication of photonic crystals for the visible spectrum by holographic lithography," Nature **404**, 53–56 (2000).
3. S. Shoji and S. Kawata, "Photofabrication of three-dimensional photonic crystals by multibeam laser interference into a photopolymerizable resin," Appl. Phys. Lett. **76**, 2668–2670 (2000).
4. T. Kondo, S. Matsuo, S. Juodkazis, and H. Misawa, "Femtosecond laser interference technique with diffractive beam splitter for fabrication of three-dimensional photonic crystals," Appl. Phys. Lett. **79**, 725–727 (2001).
5. L. Leushacke and M. Kirchner, "Three-dimensional correlation coefficient of speckle intensity for rectangular and circular apertures," J. Opt. Soc. Am. A **7**, 827–832 (1990).
6. T. Okamoto and T. Asakura, "The statistics of dynamic speckles," in *Progress in Optics, Vol. 34*, E. Wolf, ed. (Elsevier, 1995), pp. 183–248.
7. M. Kowalczyk and E. Bernabeu, "Space-time correlation properties of dynamic laser speckle in the near diffraction field of a longitudinally moving diffuse object," J. Opt. Soc. Am. A **6**, 758–764 (1989).
8. T. Yoshimura and S. Iwamoto, "Dynamic properties of three-dimensional speckles," J. Opt. Soc. Am. A **10**, 324–328 (1993).
9. H. T. Yura, S. G. Hanson, R. S. Hanson, and B. Rose, "Three-dimensional speckle dynamics in paraxial optical systems," J. Opt. Soc. Am. A **16**, 1402–1412 (1999).
10. H. T. Yura, S. G. Hanson, and M. L. Jakobsen, "Speckle dynamics resulting from multiple interfering beams," J. Opt. Soc. Am. A **25**, 318–326 (2008).
11. J. Uozumi, M. Ibrahim, and T. Asakura, "Fractal speckles," Opt. Commun. **156**, 350–358 (1998).
12. J. W. Goodman, *Speckle Phenomena in Optics* (Roberts, 2007), Chap. 3.
13. E. Kolenovic, W. Osten, and W. Juptner, "Non-linear speckle phase changes in the image plane caused by out of plane displacement," Opt. Commun. **171**, 333–344 (1999).
14. W. Kim, V. P. Safonov, V. M. Shalaev, and R. L. Armstrong, "Fractals in microcavities: giant coupled, multiplicative enhancement of optical responses," Phys. Rev. Lett. **82**, 4811–4814 (1999).
15. T. Okamoto and A. Fukuyama, "Light amplification from cantor and asymmetric multilayer resonators," Opt. Express **13**, 8122–8127 (2005).
16. J. Uozumi, "Fractality of the optical fields scattered by power-law-illuminated diffusers," Proc. SPIE **4607**, 257–267 (2001).
17. D. S. Wiersma, "The physics and applications of random lasers," Nat. Phys. **4**, 359–367 (2008).